

Short thesis for the degree of Doctor of Philosophy (PhD)

**THE ATLANTIC FORCING ON ECUADORIAN  
PALEORECORDS: SPELEOTHEMS AND TREE-RINGS**

*by*

**Danny Fernando Vargas Espin**

*Supervisor:*

**Dr. László Palcsu, PhD**



UNIVERSITY OF DEBRECEN

**Doctoral School of Physics**

Debrecen, 2023



*Prepared at*  
*the Doctoral School of Physics, University of Debrecen*  
*and the Institute for Nuclear Research*

## **1. BACKGROUND AND OBJECTIVES OF THE DOCTORAL DISSERTATION**

Paleoclimate reconstructions in tropical regions (30°N-30°S) are scarce and hindered due to the small temperature fluctuations and continuous precipitation regimes that mask the climate seasonality. However, the physical climate processes occurring at these low latitudes provide the missing elements in our understanding of the thermodynamic cycle of the Earth's past climate at high latitudes. In South America, the small number of available records are interpreted based on the changes in hydrology and not due to temperature. Most are biased towards the South American Monsoon System (SAMS), which occurs during the austral summer (DJF) and feeds the continent's central and southern parts, marking a defined onset of wet and dry seasons. However, at regions close to the equator and at the periphery of the Amazon basin, the paleoclimatological potential that can be obtained has been unexplored, perhaps due to complex seasonality dictated by the Andes topography, the rainwater bimodality brought by the Intertropical Convergence Zone (ITCZ) excursions, and lack of continuous instrumental records for the calibration of archives.

Nevertheless, these intricacies are precisely what bring the novelty and focus of this dissertation. There is an evident ambiguity in the climate literature regarding the ITCZ and SAMS boundaries, especially in Northern South America, and frequently this differentiation is vaguely stated. Long-term records harboring climate signals are required to address this ambivalence of terms, so a systematic evaluation of these systems during centennial to millennial scales is undertaken in this thesis. At the heart of this work is the development of paleoclimate reconstructions in Ecuador using terrestrial archives: speleothems, and tree-rings with the following objectives:

### **1. To evaluate the amount effect and identify the local or regional controller of the rainwater stable isotopic composition in the Ecuadorian Andes and Amazon**

In Ecuador, the rainwater stable isotopic values ( $\delta^2\text{H}_p$ ,  $\delta^{18}\text{O}_p$ ) exhibit significant local "altitude" effects due to the country's complex topography. The diverse precipitation regimes (unimodal, bimodal, and three-modal) resulting from this orography make it challenging to establish a correlation between isotopic values and local precipitation amounts. Nonetheless, stations located in these regions display similar patterns of intra-annual isotopic variability. I evaluate the hypothesis of the presence of a regional controller (V-index), which determines the main isotopic variability that is afterward

tuned by the local components. I also assess the possibility of not tagging the Ecuadorian Amazon and Andean regions as ITCZ or SAMS, but as a transition zone between these systems in a monsoon trough (Wang et al., 2017), where this regional controller is embedded. This concept is developed using Outgoing Longwave Radiation (OLR), Lagrangian back-trajectories, and a general circulation model.

## **2. To reconstruct modern centennial hydrology using $\delta^{18}\text{O}$ and $\delta^{13}\text{C}$ in cellulose from tree species**

Employing dendrochronological standard methods, tree-ring width (TRW), and cellulose-based  $\delta^{18}\text{O}_{\text{TR}}$  and  $\delta^{13}\text{C}_{\text{TR}}$  records are constructed using for the first time *Cedrela nebulosa* tree-ring species from the Amazonian lowlands. I show through spatial and spectral analysis that the wood oxygen isotopes capture a rainfall signal spatially extended in a convective hub (V-index) within the monsoon trough area. In contrast, the carbon isotopic signal is tuned to the cloudiness associated with the ITCZ excursions. These results permit us to clarify the modern chief rainfall system (SAMS or ITCZ) exerting control over Ecuador.

## **3. To reconstruct past millennial hydrology using $\delta^{18}\text{O}$ from speleothems**

Mid-Holocene paleo-precipitation reconstructions are scarce in northwestern South America. Hence, a U-Th dated speleothem from Dino cave (Dino-1) is analyzed and compared to regional records and available climate models for the epoch. A cave monitoring campaign on the site complements this work. Overall, these records allow us to assess whether recent climate patterns have also been present at the millennial scale.

## **2. MATERIALS AND METHODS**

### **2.1 Location**

The study area for both tree-rings and speleothems is located in the Mera, Province of Pastaza (1°24'S, 78°03'W, 1200 m a.s.l.) in the eastern foothills of the Ecuadorian Andes. The site is distinctive because it is a transition zone from the Amazon lowlands to the Andes with elevations above 4000 m a.s.l. The seasonal distribution of precipitation is bimodal with an average of 4500 mm annual precipitation. It consists of two dry seasons (JJA: main and DJF: minor) and two rainy seasons (MAM: main and SON: minor) (Ilbay-Yupa et al., 2021; Vuille et al., 2000). The mean annual temperature fluctuates between 21 and 23 °C.

## 2.2 Sample collection

### 2.1.1 Precipitation monitoring campaign

Monthly integrated rainwater samples were continuously collected over 48 months starting on February 2019 until January 2023 for  $\delta^2\text{H}_p$ ,  $\delta^{18}\text{O}_p$ . Samples were collected in a 12 L plastic container by adding 300 ml of paraffin oil to prevent evaporation. This follows the standard procedure for the totalizer paraffin-based method (IAEA/WMO, 2014).

### 2.1.2 Tree-ring cores

After several field campaigns, *Cedrela nebulosa* species was selected due to its prominence and visible display of rings. A total of 33 trees (67 cores) and 3 cross-sections were collected. The increment cores were mounted in wooden grooved holders with the direction of vessels vertically aligned and air-dried in the laboratory. Then, the cores were consecutively sanded up to 4000 grit enhancing tree ring visibility along with the preparation of wood anatomical features. Tree-ring width measurements were then taken using a LINTAB 6 measuring system with 0.01 mm precision and TSAP-Win software. Individual tree-ring series were imported into R statistical software and final chronology constructed using the dplR package (Bunn, 2008).

### 2.1.3 Speleothems

Three caves part of the Napo formation were explored: “Unión de los Continentes” (01° 24.4' S, 78° 2.7' W, Union hereafter), “Garganta del Dino” (01° 25.5' S, 78° 2.4 ' W, Dino hereafter) and “Copa del Mundo” (01° 24.3' S, 78° 2.6' W, Copa hereafter). The Dino cave temperature was monitored hourly with a DS1922L iButton temperature logger ( $\pm 0.5$  °C accuracy, 0.0625 °C resolution) installed at ~2 m above the ground hanging in one cave wall avoiding contact between the sensor and wall. Similarly, the air temperature outside the cave was also recorded. A complete inactive stalagmite inside Dino cave (Dino-1) was found and detached. The speleothem was cleansed, mounted, and trimmed to obtention of parallel slabs. Surfaces were consecutively grinded and polished up to 600 grit enhancing lamina visibility. This thesis focuses principally on Dino cave and its associated Dino-1 stalagmite. However, the dripwater data from Union and Copa cave was also used to complement the later-established dripwater monitoring at Dino cave. All dripwater samples were collected in 50 ml HDPE CITOTEST centrifuge tubes, labeled, packed, and shipped.

## 2.3 Analytical methods

### 2.3.1 Radioisotopes (Dating)

#### 2.3.1.1 Radiocarbon

Eighteen tree-rings were selected in the region of the “bomb-peak” for  $^{14}\text{C}$  measurements for independent validation of annual ring formation. Samples were prepared using a standard BABAB (basic-acid-basic-acid bleaching)  $\alpha$ -cellulose method (Molnár et al., 2013a). Graphite was obtained through a sealed tube graphitization method (Rinyu et al., 2013) and  $^{14}\text{C}$  measured by a MICADAS (mini carbon dating system) type AMS (Molnár et al., 2013b). The resulting percent modern carbon (pMC) values were isotope-fractionation corrected, expressed to fraction modern ( $F^{14}\text{C}$ ) and compared with the post-bomb calibration curves for the Southern Hemisphere (SH Zone 1-2 and SH Zone 3) (Hua and Barbetti, 2004; Reimer and Reimer, 2004).

#### 2.3.1.2 Uranium-Thorium

About 10 mg of drilled carbonate powder was collected in Eppendorf vials for U-Th dating from Dino-1 speleothem. Chemical preparation to separate U and Th fractions from the carbonate matrix was carried out in a Class 1000 clean laboratory, with procedures similar to those described in Edwards et al. (1987). The isotope ratio measurements were carried out on a Neptune PLUS multicollector ICP mass spectrometer equipped with an Aridus 3 desolvating system. All preparation procedures and analyses were carried out at the Isotope Climatology and Environmental Research Centre, Institute for Nuclear Research (ATOMKI) (Palcsu et al., 2022). The U-Th ages were calculated by iteration using the standard  $^{230}\text{Th}/^{238}\text{U}$  equation (Edwards et al., 1987; Kaufman and Broecker, 1965):

$$\left[ \frac{^{230}\text{Th}}{^{238}\text{U}} \right] = 1 - e^{-\lambda_{230}T} + \left( \frac{\delta^{234}\text{U}_m}{1000} \right) \times \left( \frac{\lambda_{230}}{\lambda_{230} - \lambda_{234}} \right) \times \left( 1 - e^{(\lambda_{230} - \lambda_{234})T} \right)$$

The initial  $^{234}\text{U}/^{238}\text{U}$  ratio ( $\delta^{234}\text{U}_i$ ) is calculated from:

$$\delta^{234}\text{U}_i = \delta^{234}\text{U}_m e^{\lambda_{234}T}$$

Detrital Th-corrected ages are calculated by correcting the measured  $^{230}\text{Th}/^{238}\text{U}$  ratios based on  $^{232}\text{Th}$  as an index of the initial  $^{230}\text{Th}$  contamination using the following equation (Richards and Dorale, 2003):

$$\left[ \frac{^{230}\text{Th}}{^{238}\text{U}} \right]_{\text{corr}} = \left[ \frac{^{230}\text{Th}}{^{238}\text{U}} \right] - \left[ \frac{^{232}\text{Th}}{^{238}\text{U}} \right] \times \left[ \frac{^{230}\text{Th}}{^{232}\text{Th}} \right]_i \times (e^{-\lambda_{230}T})$$

Calculated U-Th ages are reported in thousand years Before Present (ka BP), with Present defined as the year 1950 A.D. Age errors are given at  $2\sigma$ , and incorporate analytical uncertainties and uncertainties in ratios of reference materials. Finally, an age-depth model was created using the open R-package ‘‘StalAge’’ (Scholz and Hoffmann, 2011).

### 2.3.2 Stable isotopes

#### 2.3.2.1 Water

Rainwater samples were measured by a laser-based triple-liquid water isotope analyzer (T-LWIA, Los Gatos Research, Model 912-0050). The reproducibility was better than 0.16‰ for  $\delta^{18}\text{O}_p$  and better than 1.04‰ for  $\delta^2\text{H}_p$ , based on repetitions of laboratory standards.

#### 2.3.2.2 Cellulose

Four dominant and long-lived tree cores were selected and visually separated, assisted by a stereo microscope and a scalpel. The preparation of  $\alpha$ -cellulose was based on the method described by Túri et al. (2021), modified to suit tree-ring samples. Obtained cellulose samples of  $0.25 \pm 0.02$  mg were weighed into silver capsules, and subsequent isotope analysis for  $^{18}\text{O}$  and  $^{13}\text{C}$  was performed by a Thermo Finnigan DeltaPLUS XP continuous flow isotope ratio mass spectrometer. Every cellulose sample was measured at least twice for each stable isotope, and standard deviations of individual  $\delta^{13}\text{C}_{\text{TR}}$  and  $\delta^{18}\text{O}_{\text{TR}}$  measurements were  $\pm 0.1$  ‰ and  $\pm 0.35$  ‰, respectively. Results were expressed in conventional delta notation  $\delta^{18}\text{O}_{\text{TR}}$  and  $\delta^{13}\text{C}_{\text{TR}}$  relative to VSMOW and VPDB reference materials.

#### 2.3.2.3 Carbonates

Samples for stable carbon and oxygen isotopes ( $\delta^{13}\text{C}_{\text{cc}}$  and  $\delta^{18}\text{O}_{\text{cc}}$ ) were hand drilled at 5 mm spatial resolution along the central axis of Dino-1 stalagmite ( $n = 110$ ). The drilled material was weighted in Labco 12 ml glass vials for subsequent conventional analysis after digestion with  $\text{H}_3\text{PO}_4$  using an automated GasBench II sample preparation device connected to Thermo Finnigan Delta Plus XP or Thermo Scientific Delta V Plus isotope ratio mass spectrometer (Temovski et al., 2022). The obtained isotopic compositions are given as  $\delta^{13}\text{C}$  and  $\delta^{18}\text{O}$  values relative to Vienna Pee-Dee Belemnite

(VPDB) reference, with a precision better than  $\pm 0.1\%$ . In addition, a total of 28 samples were also drilled along individual growth layers at four locations for Hendy test.

## 2.4 Datasets

### *Observation/monitored*

- Precipitation and temperature
  - Puyo and Shell instrumental stations
- Rainwater stable isotopes ( $\delta^2\text{H}_p$  and  $\delta^{18}\text{O}_p$ )
  - IAEA Global Network of Isotopes in Precipitation (GNIP) database
  - Several published records

### *Gridded products*

- Precipitation and temperature
  - Climate Research Unit (CRU TS v4.05)
  - European Centre for Medium-Range Weather Forecasts (ECMWF) ERA5
  - Climate Hazard group Infrared Precipitation with Stations (CHIRPS)
  - Berkeley Earth Land/Ocean Temperature Record
- Insolation, sunshine duration, and low cloud cover
  - ModelE AR5 simulations
  - ERA5
- Outgoing Longwave Radiation (OLR)
  - NCEP-NCAR reanalysis
- Lagrangian back-trajectories
  - HYbrid Single-Parcel Lagrangian Integrated Trajectory (HYSPLIT model) with Pysplit package for visualization (Stein et al., 2015; Warner, 2018) using GDAS (Global Data Assimilation System) meteorological data

- Earth System Models (General Circulation Models)
  - Present-day gridded stable isotopologues of water from ECHAM5 atmospheric general circulation model enhanced by stable water isotope diagnostics (ECHAM5-wiso; Werner, 2019; Werner et al., 2011)
  - Global water isotopes and precipitation datasets for the mid-Holocene during austral summer (DJF) from the isotope-enabled version of the Max Planck Institute for Meteorology – Earth System Model (MPI-ESM-wiso; Cauquoin et al., 2020, 2019)
  - Precipitable water from Weather Research and Forecasting (WRF) downscaling driven by the Community Climate System Model version 4 (Chimborazo and Vuille, 2021)

## 2.5 Statistical Analysis

### *Packages*

- Wavelet – acycle MATLAB package (Li et al., 2019)
- Weighted Wavelet z-transform (WWZ) – STAR and Past software (Benn, 2012; Hammer et al., 2001; Templeton, 2004)
- Red noise – REDFIT package (Schulz and Mudelsee, 2002)
- Spatial correlations – KNMI explorer (Trouet and Van Oldenborgh, 2013).
- Climate plots – Python version 3.9.10, within the Scientific Python Development Environment (Spyder) 5.0
- Tree-ring chronology construction and analysis – dplR R package (Bunn, 2008)
- Graphical representations – R 4.3.0 , Matlab 2022 and Origin 2018

## 2.5 Reproducibility

For transparency and replicability of results, this work has been publicly archived according to the FAIR principles: Findable, Accessible, Interoperable, and Reusable and is available in the author's GitHub repository <https://github.com/vargasdanny/paleothesis>.

### 3. RESULTS

#### 3.1 Rainwater isotopic signal

- Low-level jets (Orinoco and EMTEJ) are the climate features responsible for the cross-equatorial flow from austral summer to winter (Jan-Jul) (wind arrows in Figure 1a).
- The amount of precipitation occurring at the V-index region (black box in Figure 1a) controls the precipitation isotopic signal ( $\delta^2\text{H}_p$  and  $\delta^{18}\text{O}_p$ ) downstream observed in the Ecuadorian Andes and Amazon
- The altitude effects fractionate the precipitation signal at a local scale only after the upstream convection at the V-index occurs.
- April and October are the months where the onset of the rainy season starts in the Mera study site (Figure 1b) which coincide with the lowest  $\delta^{18}\text{O}_p$  signal.
- There is poor correlation between the local amount of precipitation and the  $\delta^{18}\text{O}_p$  values.

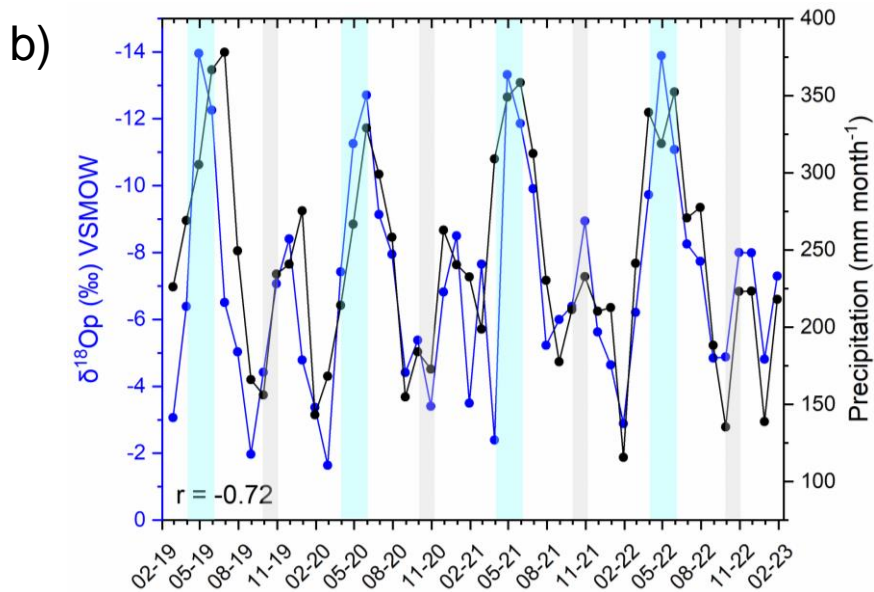
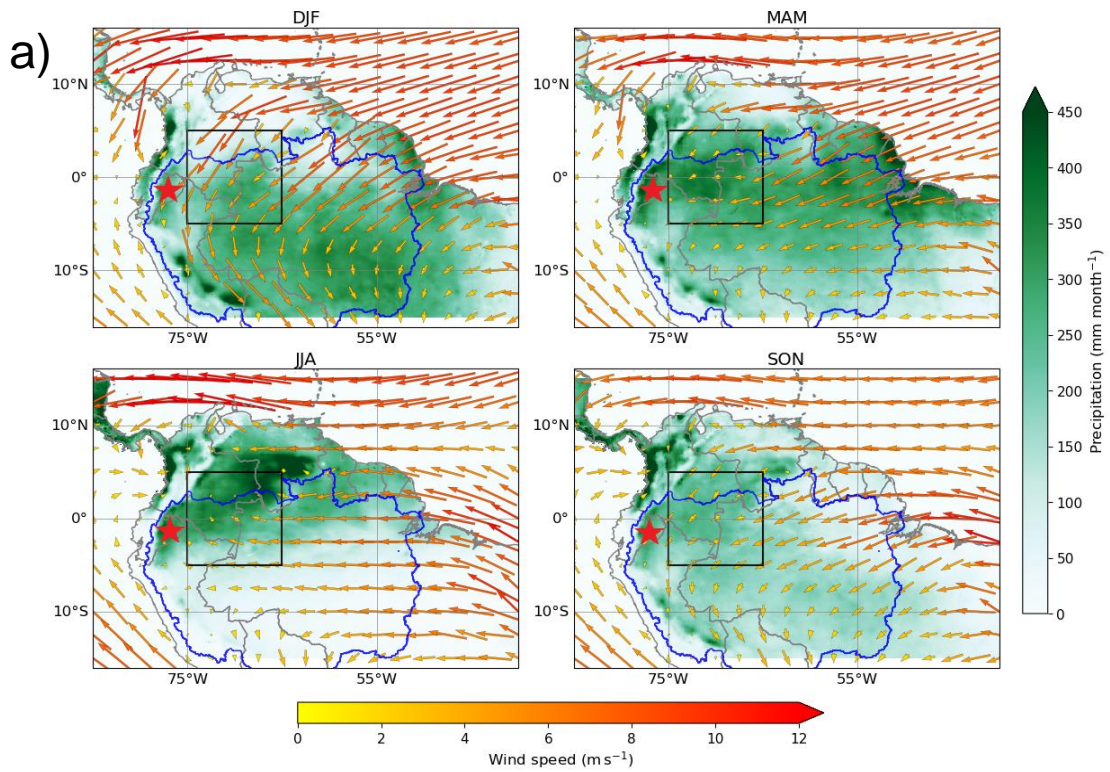


**Figure 1. a)** Plot of the 950-850 hPa ERA5 wind vectors (arrows) and mean precipitation (CHIRPS) for austral DJF (summer), MAM (autumn), JJA (winter), and SON (spring). The monsoon V-Index region over the western Amazon (5°S-5°N, 65°W-75°W) where the seasonal reversal of winds is observed is denoted by the black box. The Mera study site, central Ecuador (red star) is located within the periphery of the Amazon basin (blue line). **b)** Monthly  $\delta^{18}\text{O}_p$  in the Mera site from February 2019 to January 2023 and comparison with the amount of precipitation averaged at the V-Index region. The blue and gray stripes highlight the two peaks in precipitation during AMJ and ON. To facilitate the comparison, the left y-axis is reversed.

### 3.2 Modern climate reconstructed with tree-rings

- Obtention of the first entirely constructed tree-ring width (TRW), oxygen ( $\delta^{18}\text{O}_{\text{TR}}$ ) and carbon ( $\delta^{13}\text{C}_{\text{TR}}$ ) stable isotope records of *Cedrela nebulosa* in South America validated by radiocarbon means and spanning from 1864 to 2018 (155 years).
- Tree growth is mainly controlled by March-September local temperatures regulated by the intra-annual march of insolation.
- The  $\delta^{18}\text{O}_{\text{TR}}$  better reflects months of higher precipitation (March-June) in the western Amazon than local rainout processes at decadal time scale, owing to the strong convection in the basin at this time of the year.
- Cloud cover is an essential controller of sunshine duration, which influences the phenology of *Cedrela nebulosa*. The variability of the  $\delta^{13}\text{C}_{\text{TR}}$  is interpreted as changes in the photosynthetic rate during light-increased months (July-September) strongly regulated by cloudiness driven by the ITCZ passage.
- *Cedrela nebulosa* responds to the specific annual ITCZ excursion during March-June (wettest period) and July-September (less-wet period). Hence, during austral summer (December-February), a monsoonal rainfall mode does not influence the Ecuadorian Amazon.

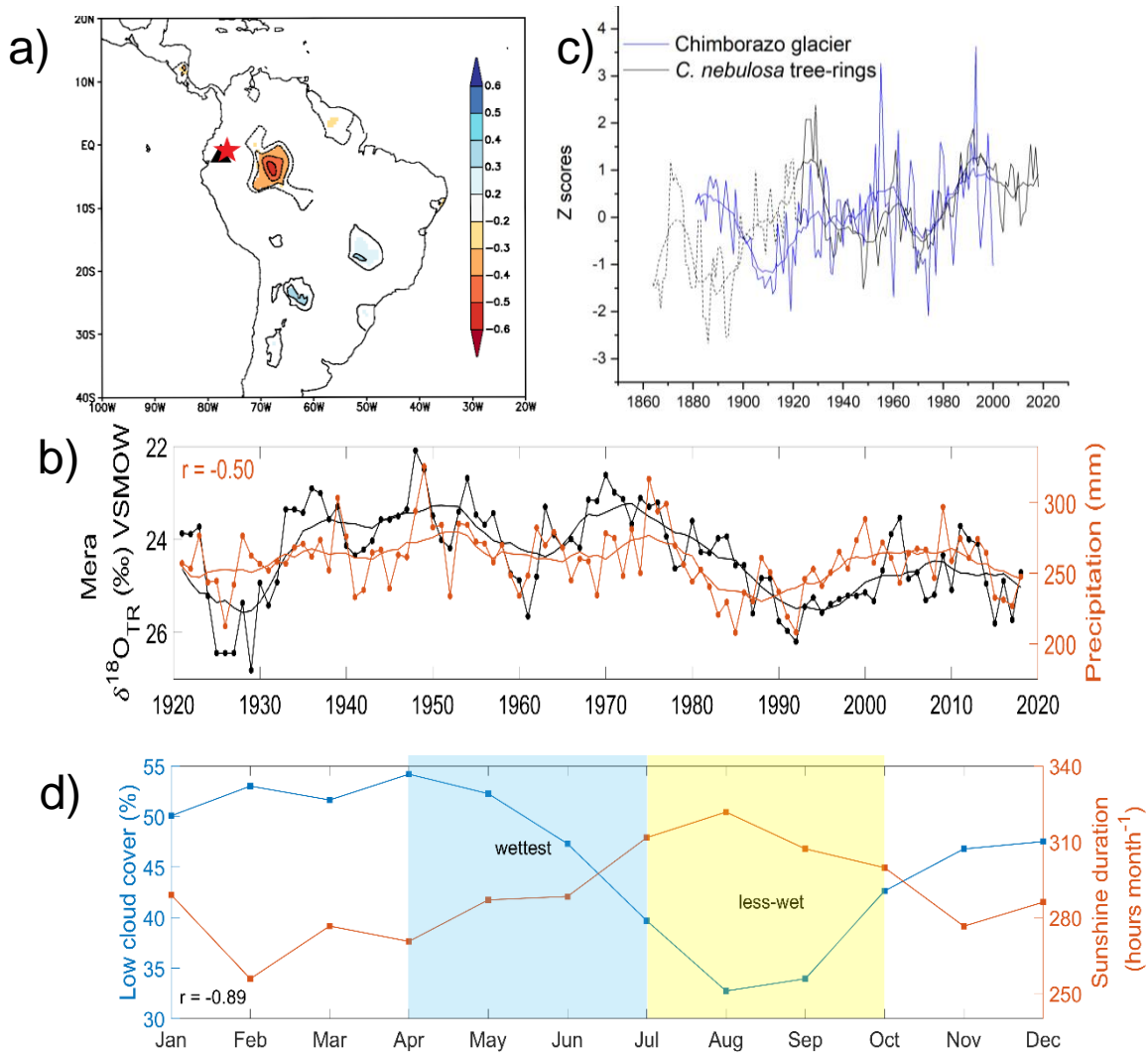


**Figure 2.** **a)** Spatial correlation fields between Mera  $\delta^{18}\text{O}_{\text{TR}}$  (red star) with regional Mar-Jun precipitation (1921-2018). The color bar indicates the strength of the correlation coefficients significant at  $p < 0.01$ . **b)** Comparison between the new Mera  $\delta^{18}\text{O}_{\text{TR}}$  record and the averaged Mar-Jun precipitation at the V-index region (orange region in a). Time-series have annual resolution and are superimposed with a 10-year Moving Average. **c)** Interdecadal comparison with Chimborazo glacier record (black triangle in a) for the period 1881-2000 smoothed with a 5-year Moving Average. **d)** Intra-annual variation of cloud cover and sunshine duration (photosynthesis controllers) in the Mera site associated with  $\delta^{13}\text{C}_{\text{TR}}$  variability.

### 3.3 Past precipitation at millennial-scale

- Monitoring of Dino cave showed that it has an almost steady temperature throughout the year ( $\sim 19.24$  °C).
- X-ray diffraction of powdered samples showed that the Dino-1 stalagmite is composed of calcite ( $\text{CaCO}_3$ ).
- U-Th dating of the Dino-1 showed that the speleothem grew from 6856 a until 5313 a, placing the record in the mid-Holocene (approximately 7 to 5 ka).
- The values of  $\delta^{18}\text{O}_{\text{cc}}$  in the record (Figure 3, red curve) varied from -6.02 to -4.53‰ VPDB (n=107), with a mean of  $-5.43 \pm 0.32$ ‰.
- The spectral analysis of the Dino-1 record (Figure 3, red curve) presents a significant 30-year period interpreted as a reflection of the Atlantic Multidecadal Oscillation signal.
- Climate simulations of total precipitation change (%) during the mid-Holocene (6.5-5.5 ka) relative to the pre-industrial period (1850 CE) reveal a progression from drier to wetter conditions in South America.
- SAMS evolved from weaker to more intense during the Holocene, whereas the ITCZ shifted southwards due to increment in the seasonal cycle of insolation over the last 7 ka in the region of the tropics (0-10°N).
- Similar coherent trends from drier to wetter conditions is observed in most of the records in northwestern South America (speleothems, lake sediments, glacier).

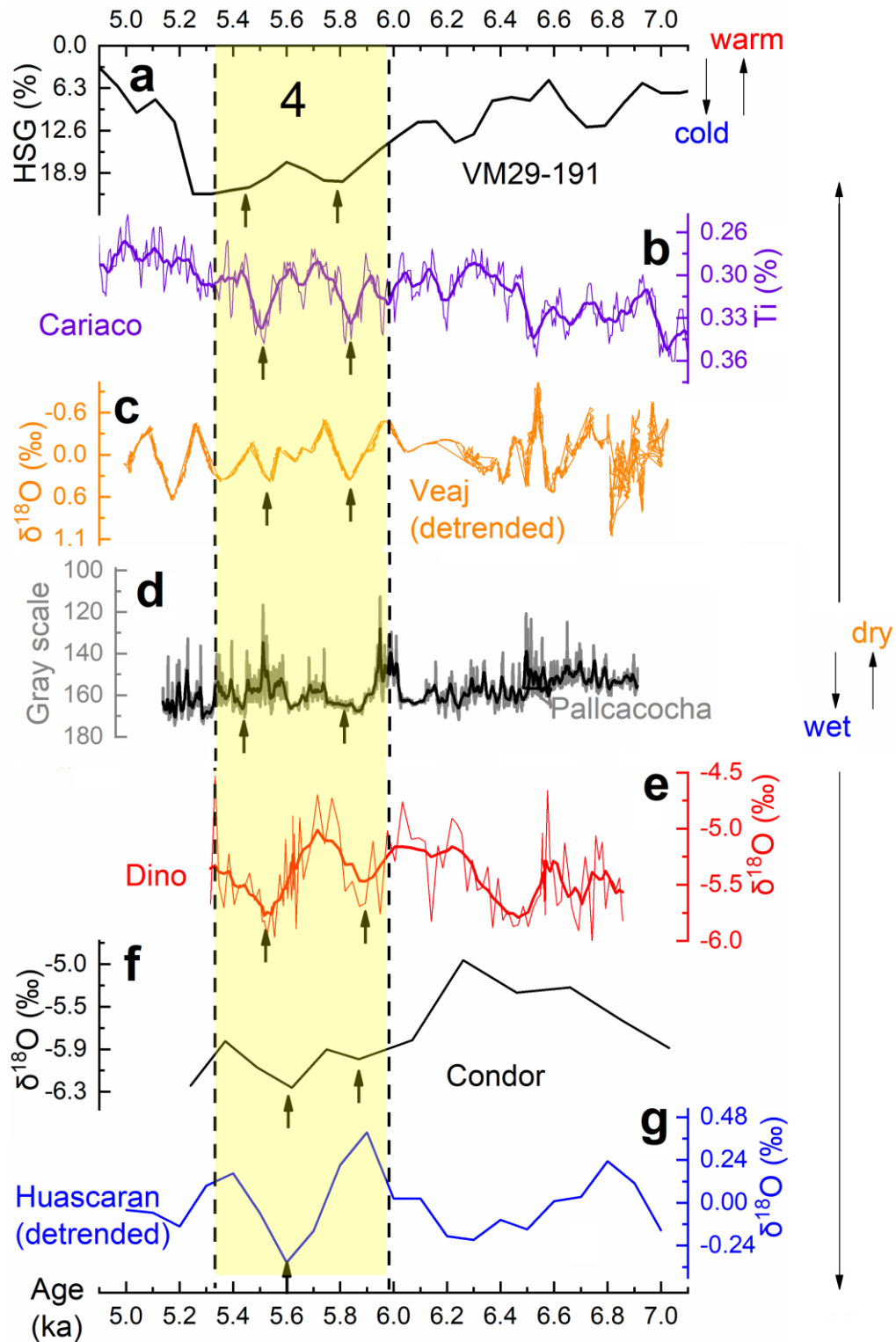


**Figure 3.** Comparison of South America mid-Holocene records spanning the period 7 to 5 ka: **a)** VM29-191 ice-rafted debris (hematite-stained grains HSG) as proxy for Bond events (Bond et al., 2001); **b)** Cariaco basin (Ven); **c)** Alfredo Jahn cave (Veaj; Ven); **d)** Pallcacocha lake sediment (Ecu) (Rodbell et al., 1999); **e)** Dino cave (Ecu, this study); **f)** Condor cave (Per); **g)** Huascarán glacier (Per). The yellow shading highlights the strong cold event (drift ice input, Bond 4) and its anomalous value shift indicated by the black arrows.

#### 4. CONCLUSIONS

In northwestern South America most records come from areas directly influenced by the South American Monsoon System (SAMS), and only a few focus on the Intertropical Convergence Zone (ITCZ) domain. This dissertation set out to investigate the past climate patterns employing tree-rings and speleothems archives near the equator where both precipitation systems converge.

The first aim of this study was to evaluate the amount effect and identify the local or regional controller of the rainwater stable isotopic composition in the Ecuadorian Andes and Amazon. The results demonstrated that moisture arrives from two primary sources: the Tropical North Atlantic (DJFM) and the South Atlantic crossing the Amazon Basin (JAS). Nevertheless, their convergence in autumn and spring (AMJ and ON) is crucial for modulating the lowest isotopic values. Precisely, this convergence is stronger at the V-Index region ( $5^{\circ}$  S– $5^{\circ}$  N,  $65^{\circ}$ – $75^{\circ}$  W), where the wind seasonality and reversal at low levels are enhanced, allowing the inter-hemispheric moisture flux transport (Figure 1). This V-index area is embedded within the ITCZ and SAMS boundaries and is called a monsoon trough globally. I propose that the amount of rainfall located at the monsoon trough, constrained at the V-Index, is a more robust approach for explaining the  $\delta^2\text{H}_p$  and  $\delta^{18}\text{O}_p$  variability rather than the local amount observed downstream.

The second objective was to reconstruct modern centennial hydrology using oxygen and carbon isotopes in cellulose from tree species. This study successfully constructed  $\delta^{18}\text{O}_{\text{TR}}$  and  $\delta^{13}\text{C}_{\text{TR}}$  records of *Cedrela nebulosa* spanning 155 years (1864-2018). The annuity of rings was independently confirmed with radiocarbon ( $^{14}\text{C}$ ) using the “bomb-pulse” (1955-2000). Spatial correlations revealed that  $\delta^{18}\text{O}_{\text{TR}}$  better reflects months of higher precipitation (March-June) in the western Amazon than local rainout processes at the decadal time scale. Two chief processes are pivotal for this climate relationship, the northward ITCZ excursion and the strong convection in the basin at this time of the year (Figure 2a-c). Similarly, this study identifies cloud cover as an essential controller of sunshine duration, which influences the phenology of *Cedrela nebulosa*. I interpreted the variability of the  $\delta^{13}\text{C}_{\text{TR}}$  as changes in the photosynthetic rate during light-increased months (July-September), regulated by cloudiness driven by the southward ITCZ passage (Figure 2e)

Finally, the third aim focused on reconstructing past millennial hydrology using  $\delta^{18}\text{O}$  from Dino-1 speleothem. The results of this study indicate that North Atlantic climate anomalies were rapidly transmitted to the tropics. In fact, Dino-1 record, although short (1.5 ka), depicts Bond event 4, one of the cold pulses that took place in the North Atlantic during the mid-Holocene. The spectral analysis of the Dino-1 record also shows a significant 30-year period which I interpret as a reflection of the Atlantic Multidecadal Oscillation signal part of its time-series variability. On a regional scale, a consistent pattern of wetness developed from early, mid-Holocene, and pre-Industrial times observed in climate models and northeastern and northwestern regional speleothem, sediments, and glacier records.

## **5. NEW SCIENTIFIC FINDINGS**

### **Rainwater stable isotopes**

- The validation of the existence of a regional convection hub at  $5^{\circ}\text{S}$ - $5^{\circ}\text{N}$ ,  $65^{\circ}\text{W}$ - $75^{\circ}\text{W}$  (V-index, Wang and Fu, 2002) located in the monsoon trough that controls the primary isotopic signal in precipitation through the amount effect. This V-index region can be considered an aerial lake containing high precipitable water (Arraut et al., 2012).
- The North and South Atlantic moisture source and the altitude effect due to the Andes orography are the complementary effects tuning the local isotopic signal.
- The moisture arriving at the western Ecuadorian Amazon and Andes is carried by two low-level jets: Orinoco (950–800 hPa) and the Equatorial mid-tropospheric easterly jet (700–600 hPa), which are SAMS features.
- The new local meteoric water line for the Mera site (western Amazon) is  $\delta^2\text{H} = 8.33\delta^{18}\text{O} + 14.99$ .
- The mean annual temperature is  $18.97^{\circ}\text{C}$  in the study site, except for an  $\sim 1^{\circ}$  drop in July-August related to the reduced insolation (June solstice).

### **Tree-rings and modern climate**

- First dendroclimatological study in Ecuador and Northern South America to show the ITCZ imprint in a tree-ring archive.
- The key feature for identifying *Cedrela nebulosa* rings is the presence of embedded big pores and vessels in marginal parenchyma at the beginning of the growing season.
- $\delta^{18}\text{O}_{\text{TR}}$  reflects the ITCZ passage over the western Amazon during the wettest months (March–June).
- $\delta^{13}\text{C}_{\text{TR}}$  reflects changes in the photosynthetic rate during light-increased months (July–September) with low cloudiness.
- *C. nebulosa* is well-adapted to wet environments presenting one distinct season of higher precipitation during the year.

### **Speleothem and mid-Holocene climate**

- The mid-Holocene climate was wetter than the early Holocene but drier than pre-Industrial in northwestern South America due to ITCZ latitudinal southward shift.
- Dino-1 speleothem record presents a significant 30-year periodicity associated with the Atlantic Meridional Overturning Circulation (AMOC).
- Dino-1 speleothem record is a good proxy for mid-Holocene hydrology and seems to register Bond event 4, a strong cold pulse over the North Atlantic observed in northwestern tropical records.

## 6. REFERENCES

- Arraut, J.M., Nobre, C., Barbosa, H.M.J., Obregon, G., Marengo, J., 2012. Aerial Rivers and Lakes: Looking at Large-Scale Moisture Transport and Its Relation to Amazonia and to Subtropical Rainfall in South America. *J. Clim.* 25, 543–556. <https://doi.org/10.1175/2011JCLI4189.1>
- Benn, D., 2012. Algorithms+ Observations= VStar. *J. Am. Assoc. Var. Star Obs.* 40, 852.
- Bond, G., Kromer, B., Beer, J., Muscheler, R., Evans, M.N., Showers, W., Hoffmann, S., Lotti-Bond, R., Hajdas, I., Bonani, G., 2001. Persistent solar influence on north atlantic climate during the Holocene. *Science* (80-. ). 294, 2130 – 2136. <https://doi.org/10.1126/science.1065680>
- Bunn, A.G., 2008. A dendrochronology program library in R (dplR). *Dendrochronologia* 26, 115–124. <https://doi.org/10.1016/j.dendro.2008.01.002>
- Cauquoin, A., Werner, M., Lohmann, G., 2020. MPI-ESM-wiso simulations data for preindustrial and mid-Holocene conditions. <https://doi.org/10.1594/PANGAEA.912258>
- Cauquoin, A., Werner, M., Lohmann, G., 2019. Water isotopes -- climate relationships for the mid-Holocene and preindustrial period simulated with an isotope-enabled version of MPI-ESM. *Clim. Past* 15, 1913–1937. <https://doi.org/10.5194/cp-15-1913-2019>
- Chimborazo, O., Vuille, M., 2021. Present-day climate and projected future temperature and precipitation changes in Ecuador. *Theor. Appl. Climatol.* 143, 1581–1597. <https://doi.org/10.1007/s00704-020-03483-y>
- Edwards, L., Chen, J.H., Wasserburg, G.J., 1987. <sup>238</sup>U-<sup>234</sup>U-<sup>230</sup>Th-<sup>232</sup>Th systematics and the precise measurement of time over the past 500,000 years. *Earth Planet. Sci. Lett.* 81, 175–192. [https://doi.org/10.1016/0012-821X\(87\)90154-3](https://doi.org/10.1016/0012-821X(87)90154-3)
- Hammer, Ø., Harper, D., Ryan, P., 2001. PAST: Paleontological Statistics Software package for Education and Data Analysis. *Palaeontol. Electron.* 4, 1–9.
- Hua, Q., Barbetti, M., 2004. Review of tropospheric bomb <sup>14</sup>C data for carbon cycle modeling and age calibration purposes. *Radiocarbon* 46, 1273–1298. <https://doi.org/10.1017/S0033822200033142>
- IAEA/WMO, 2014. Precipitation Sampling guide V2. 02 September 2014.
- Ilbay-Yupa, M., Lavado-Casimiro, W., Rau, P., Zubieta, R., Castellón, F., 2021. Updating regionalization of precipitation in Ecuador. *Theor. Appl. Climatol.* 143, 1513–1528. <https://doi.org/10.1007/s00704-020-03476-x>
- Li, M., Hinnov, L., Kump, L., 2019. Acycle: Time-series analysis software for paleoclimate research and education. *Comput. Geosci.* 127, 12–22. <https://doi.org/10.1016/j.cageo.2019.02.011>
- Molnár, M., Janovics, R., Major, I., Orsovsvzki, J., Gönczi, R., Veres, M., Leonard, A.G., Castle, S.M., Lange, T.E., Wacker, L., Hajdas, I., Jull, A.J.T., 2013a. Status Report of the New AMS <sup>14</sup>C Sample Preparation Lab of the Hertelendi Laboratory of Environmental Studies (Debrecen, Hungary). *Radiocarbon* 55, 665–676. [https://doi.org/10.2458/azu\\_js\\_rc.55.16394](https://doi.org/10.2458/azu_js_rc.55.16394)
- Molnár, M., Rinyu, L., Veres, M., Seiler, M., Wacker, L., Synal, H.-A., 2013b. EnvironMICADAS: A Mini <sup>14</sup>C AMS with Enhanced Gas Ion Source Interface in the Hertelendi Laboratory of Environmental Studies (HEKAL), Hungary. *Radiocarbon* 55, 338–344. <https://doi.org/10.1017/S0033822200057453>
- Palcsu, L., Temovski, M., Vargas, D., Kiss, G.I., Surányi, G., 2022. A new U-Th laboratory for dating speleothems, in: *Climate Change: The Karst Record IX (KR9)*. p. 120.
- Reimer, P.J., Reimer, R., 2004. CALIBomb radiocarbon calibration. *Interact. Progr.*

- available on-line <http://intcal.qub.ac.uk/CALIBomb/frameset.html>.
- Richards, D.A., Dorale, J.A., 2003. Uranium-series Chronology and Environmental Applications of Speleothems. *Rev. Mineral. Geochemistry* 52, 407–460. <https://doi.org/10.2113/0520407>
- Rinyu, L., Molnár, M., Major, I., Nagy, T., Veres, M., Kimák, Á., Wacker, L., Synal, H.-A., 2013. Optimization of Sealed Tube Graphitization Method for Environmental C-14 Studies Using MICADAS. *Nucl. Instruments Methods Phys. Res. Sect. B Beam Interact. with Mater. Atoms* 294, 270–275. <https://doi.org/10.1016/j.nimb.2012.08.042>
- Rodbell, D.T., Seltzer, G.O., Anderson, D.M., Abbott, M.B., Enfield, D.B., Newman, J.H., 1999. An ~15,000-Year Record of El Niño-Driven Alluviation in Southwestern Ecuador. *Science* (80-. ). 283, 516–520. <https://doi.org/10.1126/science.283.5401.516>
- Scholz, D., Hoffmann, D.L., 2011. StalAge – An algorithm designed for construction of speleothem age models. *Quat. Geochronol.* 6, 369–382. <https://doi.org/10.1016/j.quageo.2011.02.002>
- Schulz, M., Mudelsee, M., 2002. REDFIT: estimating red-noise spectra directly from unevenly spaced paleoclimatic time series. *Comput. Geosci.* 28, 421–426. [https://doi.org/https://doi.org/10.1016/S0098-3004\(01\)00044-9](https://doi.org/https://doi.org/10.1016/S0098-3004(01)00044-9)
- Stein, A.F., Draxler, R.R., Rolph, G.D., Stunder, B.J.B., Cohen, M.D., Ngan, F., 2015. NOAA’s HYSPLIT Atmospheric Transport and Dispersion Modeling System. *Bull. Am. Meteorol. Soc.* 96, 2059–2077. <https://doi.org/10.1175/BAMS-D-14-00110.1>
- Templeton, M., 2004. Time-series analysis of variable star data. *J. Am. Assoc. Var. Star Obs.* vol. 32, no. 1, p. 41-54 32, 41–54.
- Trouet, V., Van Oldenborgh, G.J., 2013. KNMI Climate Explorer: A Web-Based Research Tool for High-Resolution Paleoclimatology. *Tree-Ring Res.* 69, 3–13. <https://doi.org/10.3959/1536-1098-69.1.3>
- Túri, M., Hubay, K., Molnár, M., Braun, M., László, E., Futó, I., Palcsu, L., 2021. Holocene paleoclimate inferred from stable isotope ( $\delta^{18}\text{O}$  and  $\delta^{13}\text{C}$ ) values in Sphagnum cellulose, Mohos peat bog, Romania. *J. Paleolimnol.* 66, 229–248. <https://doi.org/10.1007/s10933-021-00202-z>
- Vuille, M., Bradley, R.S., Keimig, F., 2000. Climate Variability in the Andes of Ecuador and Its Relation to Tropical Pacific and Atlantic Sea Surface Temperature Anomalies. *J. Clim.* 13, 2520–2535. [https://doi.org/10.1175/1520-0442\(2000\)013<2520:CVITAO>2.0.CO;2](https://doi.org/10.1175/1520-0442(2000)013<2520:CVITAO>2.0.CO;2)
- Wang, H., Fu, R., 2002. Cross-Equatorial Flow and Seasonal Cycle of Precipitation over South America. *J. Clim.* 15, 1591–1608. [https://doi.org/10.1175/1520-0442\(2002\)015<1591:CEFASC>2.0.CO;2](https://doi.org/10.1175/1520-0442(2002)015<1591:CEFASC>2.0.CO;2)
- Wang, P.X., Wang, B., Cheng, H., Fasullo, J., Guo, Z., Kiefer, T., Liu, Z., 2017. The global monsoon across time scales: Mechanisms and outstanding issues. *Earth-Science Rev.* 174, 84–121. <https://doi.org/10.1016/j.earscirev.2017.07.006>
- Warner, M.S.C., 2018. Introduction to PySPLIT: A Python Toolkit for NOAA ARL’s HYSPLIT Model. *Comput. Sci. Eng.* 20, 47–62. <https://doi.org/10.1109/MCSE.2017.3301549>
- Werner, M., 2019. ECHAM5-wiso simulation data - present-day, mid-Holocene, and Last Glacial Maximum. <https://doi.org/10.1594/PANGAEA.902347>
- Werner, M., Langebroek, P.M., Carlsen, T., Herold, M., Lohmann, G., 2011. Stable water isotopes in the ECHAM5 general circulation model: Toward high-resolution isotope modeling on a global scale. *J. Geophys. Res.* 116, D15109. <https://doi.org/10.1029/2011JD015681>

## 7. PUBLICATIONS IN THE TOPIC OF THE DISSERTATION



UNIVERSITY of  
DEBRECEN

UNIVERSITY AND NATIONAL LIBRARY  
UNIVERSITY OF DEBRECEN

H-4002 Egyetem tér 1, Debrecen

Phone: +3652/410-443, email: publikaciok@lib.unideb.hu

Registry number: DEENK/109/2023.PL  
Subject: PhD Publication List

Candidate: Danny Fernando Vargas Espin  
Doctoral School: Doctoral School of Physics  
MTMT ID: 10080878

### List of publications related to the dissertation

#### Foreign language scientific articles in international journals (2)

1. **Vargas Espin, D. F.**, Pucha-Cofrep, D., Serrano-Vincenti, S., Burneo, A., Carlosama, L., Herrera, M., Cerna, M., Molnár, M., Jull, A. J. T., Temovski, M., László, E., Futó, I., Horváth, A., Palcsu, L.: ITCZ precipitation and cloud cover excursions control Cedrela nebulosa tree-ring oxygen and carbon isotopes in the northwestern Amazon. *Glob. Planet. Change*. 211, 1-15, 2022. ISSN: 0921-8181. DOI: <http://dx.doi.org/10.1016/j.gloplacha.2022.103791> IF: 4.956 (2021)
2. **Vargas Espin, D. F.**, Chimborazo, O., László, E., Temovski, M., Palcsu, L.: Rainwater Isotopic Composition in the Ecuadorian Andes and Amazon Reflects Cross-Equatorial Flow Seasonality. *Water*. 14 (13), 1-22, 2022. EISSN: 2073-4441. DOI: <https://doi.org/10.3390/w14132121> IF: 3.53 (2021)

#### Foreign language abstracts (4)

3. **Vargas Espin, D. F.**, Temovski, M., László, E., Kiss, G. I., Palcsu, L.: Middle Holocene ITCZ shifts: Evidence from Central Ecuador. In: *Climate Change : The Karst Record IX (KR9): Programme and abstract*. Eds.: Gina Moseley, Linda Partl, Paul Töchterle, Gabriella Koltai, Mojgan Soleimani, Jonathan Baker, Christoph Spötl, University of Innsbruck, Innsbruck, 102, 2022.
4. **Vargas Espin, D. F.**, Temovski, M., Kiss, G. I., László, E., Surányi, G., Palcsu, L.: Preliminary results of speleothem U-Th dating and paleoclimate reconstruction from Garganta del Dicho Cave (Ecuador). In: *28th International Karstological School "Classical karst" Regional karstology - local and general aspects*. Ed.: Matej Blatnik, Franci Gabrovšek, Cyril Mayaud, Andrej Minevc, Metka Petrič, Nataša Ravbar, Nadja Zupan Hajna, Založba ZRC, Ljubljana, 133, 2021. ISBN: 9789610505617





5. **Vargas Espin, D. F.**, Pucha-Cofrep, D., Burneo, A., Carlosama, L., Herrera, M., Serrano, S., Cerna, M., Jull, A. J. T., Molnár, M., Futó, I., Horváth, A., Temovski, M., Palcsu, L.: Impact of cloud coverage on growth dynamics of *Cedrela nebulosa* from an Amazonian pre-montane forest in Central Ecuador.  
In: CL1.24 Interdisciplinary Tree-ring research. Ed.: Kerstin Treydte, Flurin Babst, Giovanna Battipaglia, Jan Esper, EGU General Assembly, [Vienna], 1, 2020.
6. **Vargas Espin, D. F.**, Temovski, M., László, E., Palcsu, L.: Paleoclimate reconstruction based on speleothems from Ecuadorian caves.  
In: 27th International Karstological School "Classical karst" Karst hydrogeology - research trends and applications : Abstracts & Guide Book. Ed.: Matej Blatnik, Franci Gabrovšek, Blaž Kogovšek, Cyril Mayaud, Metka Petrič, Nataša Ravbar, Založba ZRC, Ljubljana, 133-134, 2019. ISBN: 9789610501961

### List of other publications

#### Foreign language abstracts (2)

7. Palcsu, L., Temovski, M., **Vargas Espin, D. F.**, Kiss, G. I., Surányi, G.: A new U-Th laboratory for dating speleothems.  
In: Climate Change : The Karst Record IX (KR9): Programme and abstract. Eds.: Gina Moseley, Linda Partl, Paul Töchterle, Gabriella Koltai, Mojgan Soleimani, Jonathan Baker, Christoph Spötl, University of Innsbruck, Innsbruck, 120, 2022.
8. Temovski, M., Molnár, K., **Vargas Espin, D. F.**, Kiss, G. I., Palcsu, L.: Petrographic and geochemical properties of a subaqueous speleothem from a Macedonian cave-preliminary results and insight into MIS 7 paleoclimate record of the Balkan Peninsula.  
In: Climate Change : The Karst Record IX (KR9): Programme and abstract. Eds.: Gina Moseley, Linda Partl, Paul Töchterle, Gabriella Koltai, Mojgan Soleimani, Jonathan Baker, Christoph Spötl, University of Innsbruck, Innsbruck, 106-107, 2022.

**Total IF of journals (all publications): 8,486**

**Total IF of journals (publications related to the dissertation): 8,486**

The Candidate's publication data submitted to the iDEa Tudóstér have been validated by DEENK on the basis of the Journal Citation Report (Impact Factor) database.

13 April, 2023

